Electronic structure of dye-sensitized TiO_2 clusters from many-body perturbation theory

Noa Marom,[1,*] Jonathan E. Moussa,[1] Xinguo Ren,[2] Alexandre Tkatchenko,[2] and James R. Chelikowsky[1,3]

[1]*Center for Computational Materials, Institute for Computational Engineering and Sciences, The University of Texas at Austin, Austin, Texas 78712, USA*

[2]*Fritz-Haber-Institut der Max-Planck-Gesellschaft, Faradayweg 4-6, 14195, Berlin, Germany*

[3]*Departments of Physics and Chemical Engineering, The University of Texas at Austin, Austin, Texas 78712, USA*

(Received 9 August 2011; revised manuscript received 15 October 2011; published 13 December 2011)

The development of new types of solar cells is driven by the need for clean and sustainable energy. In this respect dye-sensitized solar cells (DSC) are considered as a promising route for departing from the traditional solid state cells. The physical insight provided by computational modeling may help develop improved DSCs. To this end, it is important to obtain an accurate description of the electronic structure, including the fundamental gaps and level alignment at the dye-TiO_2 interface. This requires a treatment beyond ground-state density functional theory (DFT). We present a many-body perturbation theory study, within the G_0W_0 approximation, of two of the crystalline phases of dye-sensitized TiO_2 clusters, reported by Benedict and Coppens, [J. Am. Chem. Soc. **132**, 2938 (2010)]. We obtain geometries in good agreement with the experiment by using DFT with the Tkatchenko-Scheffler van der Waals correction. We demonstrate that even when DFT gives a good description of the valence spectrum and a qualitatively correct picture of the electronic structure of the dye-TiO_2 interface, G_0W_0 calculations yield more valuable quantitative information regarding the fundamental gaps and level alignment. In addition, we systematically investigate the issues pertaining to G_0W_0 calculations, namely: (i) convergence with respect to the number of basis functions, (ii) dependence on the mean-field starting point, and (iii) the validity of the assumption that the DFT wave function is a good approximation to the quasiparticle wave function. We show how these issues are manifested for dye molecules and for dye-sensitized TiO_2 clusters.

DOI: 10.1103/PhysRevB.84.245115 PACS number(s): 73.22.−f

I. INTRODUCTION

The development of new types of solar cells is driven by the need for clean, sustainable energy. One promising route for departing from the traditional solid-state cells is a dye-sensitized solar cell (DSC).[1,2] In this type of cell, the light is harvested by a sensitizer, which may be a dye molecule or a semiconductor quantum dot,[3] attached to a wide-band-gap semiconductor of mesoporous or nanocrystalline morphology, typically TiO_2. Charge separation occurs via electron injection from the photoexcited sensitizer into the oxide.[1,2] This can happen either indirectly, by electron transfer from the excited state of the dye to the conduction band of the oxide, or directly, through a charge-transfer excitation. The injected electrons subsequently migrate to the collector electrode, and the dye is regenerated by electron donation from an organic hole conductor or an electrolyte.

DSCs have achieved efficiencies exceeding 11%[1,4] and are still far from their theoretical limit, as compared to the more technologically mature solid-state cells.[5] One actively pursued research avenue toward improving the performance and reducing the cost of DSCs is the synthesis of new dyes. Specifically, there is an interest in dyes with a smaller gap that can maximally utilize the solar spectrum and in fully organic dyes without expensive transition metals. The physical insight provided by computational modeling may help engineer new dyes and assess their performance.

Many electronic structure calculations have been done for various dye molecules (see, e.g., Refs. 4 and 6), typically employing density functional theory (DFT) for the ground-state properties and time-dependent DFT (TDDFT) for the absorption spectrum. However, the efficiency of electron injection depends not only on the dye molecule itself but also on its interface with the TiO_2. The interaction between the dye and the TiO_2 leads to changes in their relative energy level alignment and to hybridization of their molecular orbitals. To capture this, the combined dye+TiO_2 system has to be treated as a whole. Such studies are scarce owing to the size and complexity of the combined system. The few studies reported thus far[7–9] have employed TDDFT with conventional semilocal and hybrid functionals.

Like DFT, TDDFT is exact in principle[10,11] but still suffers from the deficiencies of commonly used approximations to the exchange-correlation (xc) functional, e.g., the incorrect derivative discontinuity and self-interaction errors (SIE).[12] These affect the description of the ground state and of excited states. For example, SIE have been shown to lead to an unsatisfactory description of the ground-state electronic structure of transition metal phthalocyanines,[13,14] which are chemically similar to commonly used dyes. Indeed, TDDFT has been shown to provide an inconsistent description of the absorption spectrum of porphyrins and large extended π-systems.[15] Problems stemming from the xc-functional also lead to difficulties in the description of charge-transfer excitations when TDDFT is used with standard functionals, including conventional hybrids.[16] Recently, a successful treatment of charge-transfer excitations in coumarine-based dyes has been achieved by using TDDFT with a range-separated hybrid functional, where the range separation parameter is tuned to a system-specific value.[17] However, even this method is not guaranteed to succeed for dye-sensitized TiO_2 because, as is often the case for interfaces between dissimilar materials, the two sides of the interface may require different fractions of exact exchange (Exx) and different range-separation parameters.

An alternative route to calculating the optical absorption spectrum is through Green's function-based many-body perturbation theory.[18,19] Within this approach quasiparticle (QP) excitation energies are obtained via the GW approximation, where G is the one-particle Green's function and W is the dynamically screened Coulomb potential. On the basis of GW, one may construct the two-particle Green's function, which describes coupled electron-hole excitations, and then solve the Bethe-Salpeter equation (BSE)[11,20] to obtain the optical spectrum. The GW + BSE approach has been applied successfully to obtain the optical spectra of several molecular systems[21–23] and of TiO_2;[24] therefore, it is a promising method for treating dye-sensitized TiO_2.

Importantly, the success of a BSE calculation is contingent upon a reliable underlying GW calculation. Owing to the exceedingly high computational cost of fully self-consistent GW,[25,26] a perturbative approach is often taken, where QP excitation energies are obtained as a first-order correction to the DFT eigenvalues, based on the underlying single-electron DFT orbitals. This approach, which is also used here, is known as G_0W_0. The main issues pertaining to G_0W_0 calculations, further elaborated below, are (i) convergence with respect to the number of basis functions, (ii) sensitivity to the mean-field starting point, and (iii) the validity of the assumption that the DFT wave function is a good approximation to the QP wave function. Consequently, there is a need to examine the feasibility and performance of G_0W_0 for the valence spectrum, fundamental gaps, and level alignment of dye-sensitized TiO_2.

In order to assess the performance of computational methods, a direct comparison to experiment is essential. Unfortunately, it is often the case that the structure of the dye+TiO_2 system is not known exactly, owing to the difficulty in performing precise experimental measurements of the geometry of disordered interfaces. In such a situation it is difficult to determine whether discrepancies between theory and experiment arise from the limitations of the computational methods used or simply from assuming an incorrect geometry. Conversely, broadening of photoemission and adsorption spectra may limit the ability to pin down meaningful differences between theory and experiment. Therefore, we must carefully choose a test system for the purpose of method validation.

Recently, Benedict and Coppens reported several crystalline phases of dye-sensitized TiO_2 clusters.[27] These systems have a well-defined structure, characterized by x-ray diffraction (XRD). This, as well as the absence of solvent and counterions, makes them an ideal test bed for theory because a direct comparison to the experiment is possible. For the purpose of this study, we have chosen two of these systems, schematically depicted in Fig. 1: (i) Ti_2cat_2, whose unit cell contains four units of $C_{30}H_{52}O_{10}Ti_2$—a $(TiO_2)_2$ cluster sensitized with two molecules of catechol (cat) and capped with six additional molecules of isopropyl alcohol (IPA)—a total of 376 atoms, 94 in each molecular unit; (ii) Ti_3INA_3, whose unit cell contains two units of $C_{39}H_{61}N_3O_{14}Ti_3$—a $(TiO_2)_3$ cluster sensitized with three molecules of isonicotinic acid (INA) and capped with seven additional molecules of IPA—a total of 240 atoms, 120 in each molecular unit.

Ti_2cat_2 and Ti_3INA_3, though obviously much smaller than the dye molecules and TiO_2 particles used in actual DSCs, contain all the essential physics of the local interaction between the dye and the TiO_2 clusters, i.e., the level alignment and the orbital hybridization between the two. Although the fundamental gaps of the TiO_2 clusters modeled here are much wider than those of the larger bulklike nanoparticles used in DSCs, the principles demonstrated here, particularly with respect to method validation, will still apply when it comes to the description of larger systems. Screening effects, which are present in extended systems, are not accounted for here.

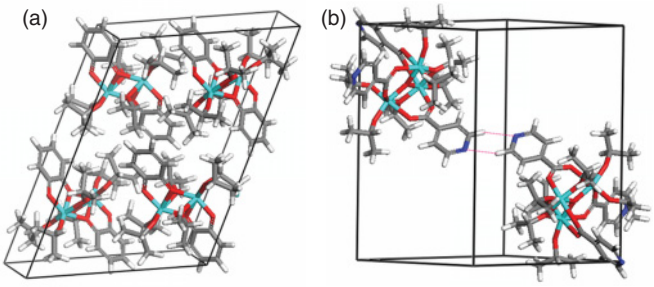

FIG. 1. (Color online) Schematic illustration of the crystal structures of (a) Ti_2cat_2 and (b) Ti_3INA_3 (Ti-cyan/light gray, O-red/dark gray, C-gray, N-blue/medium gray, H-white). The N···H hydrogen bond in Ti_3INA_3 is indicated in (b).

We present a benchmark GW study of dye-sensitized TiO_2 clusters. We demonstrate that even when DFT gives a good description of the valence spectrum and a qualitatively correct picture of the electronic structure of the dye-TiO_2 interface, G_0W_0 calculations yield more valuable quantitative information regarding the fundamental gaps and level alignment. We then discuss the level alignment of Ti_2cat_2 and Ti_3INA_3, in the context of DSCs. In addition, we systematically investigate the issues pertaining to G_0W_0 calculations, namely: (i) convergence with respect to the number of basis functions, (ii) sensitivity to the mean-field starting point, and (iii) the validity of the assumption that the DFT wave function is a good approximation to the QP wave function. We show how these issues are manifested for dye molecules and for dye-sensitized TiO_2 clusters.

II. METHODS

All calculations were performed using the all-electron numeric atom-centered orbital (NAO) code, FHI-aims.[28,29] The NAO basis sets are grouped into a minimal basis, containing only basis functions for the core and valence electrons of the free atom, followed by four hierarchically constructed tiers of additional basis functions (tier 1–4). Geometry relaxations were carried out using the generalized gradient approximation (GGA) of Perdew, Burke, and Ernzerhof (PBE)[30] with a tier 2 basis set, which has been demonstrated to approach the basis set limit for ground-state GGA calculations and be nearly free of basis set superposition errors (BSSE).[28] The Tkatchenko-Scheffler (TS) van der Waals (vdW) correction[31] was used to treat dispersion interactions. A detailed account is given in Appendix.

The QP energy levels were computed using the G_0W_0 method. In this approach QP energies are obtained perturbatively as a first-order correction to the Kohn-Sham (KS) DFT eigenvalues, employing the diagonal approximation to the self-energy. This amounts to assuming that the orbitals

obtained from the DFT calculations mimic the quasiparticle wave function sufficiently well, in which case only the orbital energies need to be corrected.[18] Although this approximation is not universally valid (see, e.g., Ref. 22), it often yields excellent results. A complete account of the all-electron implementation of G_0W_0 in FHI-aims has been given elsewhere.[32] Briefly, the implementation makes use of the resolution-of-identity (RI) technique, whereby a set of auxiliary basis functions is introduced to represent both the Coulomb potential and the noninteracting response function. This allows for efficient GW calculations with NAO basis functions. The RI accuracy and NAO basis set convergence have been benchmarked in Ref. 32. The self-energy is first calculated on the imaginary frequency axis and then analytically continued to the real frequency axis using a two-pole fitting procedure.[33] The NAO basis set convergence of G_0W_0 calculations is further examined below.

Performing GW calculations in an all-electron code has the advantage that no pseudopotential errors are introduced.[26,34] In addition, using NAO basis functions has been observed to lead to a more rapid convergence with the number of basis functions, as compared to plane waves, because NAOs are inherently localized over regions of large electron density, in contrast to delocalized plane waves. The fact that periodic boundary conditions are not imposed in FHI-aims is another advantage for GW calculations of molecular systems, as there is no need for large regions of vacuum to avoid artifacts from spurious interactions between periodic replicas.

In order to examine the starting point dependence of G_0W_0 and find an optimal starting point, G_0W_0 calculations were carried out from different mean-field starting points. These include PBE, the one-parameter PBE-based hybrid functional (PBEh),[35] PBE with a varying fraction of exact exchange (Exx), and Hartree-Fock (HF). The name "PBEh" is reserved for PBE with 25% exact exchange. Functionals with a different fraction of exact exchange are denoted as, e.g., PBE+35%Exx. G_0W_0 calculations are denoted as GW@[mean-field starting point]. For example, GW@PBE denotes a G_0W_0 calculation on top of a PBE DFT calculation. The scaled zero-order regular approximation (ZORA) method[36] was used to account for scalar relativistic effects in the single-point DFT calculations that served as starting points for G_0W_0.

III. RESULTS AND DISCUSSION

A. Basis Set Convergence

We begin by verifying the basis set convergence of our G_0W_0 calculations. The standard implementation of the G_0W_0 self-energy contains an infinite sum over states, which in practice translates into a finite sum over a very large number of occupied and unoccupied states. This leads to a notoriously slow convergence of such calculations with respect to basis set size.[37] Owing to the size of Ti_2cat_2 and Ti_3INA_3 the basis set convergence studies were conducted for smaller fragments of the full systems, shown in Fig. 2: a TiO_2 molecule, catechol, and IPA. In Fig. 3, the QP highest occupied molecular orbital (HOMO) and lowest unoccupied molecular orbital (LUMO), calculated based on PBE and PBEh with increasingly large basis sets are compared to experimental ionization potentials (IP) and electron affinities (EA), respectively. QP energies

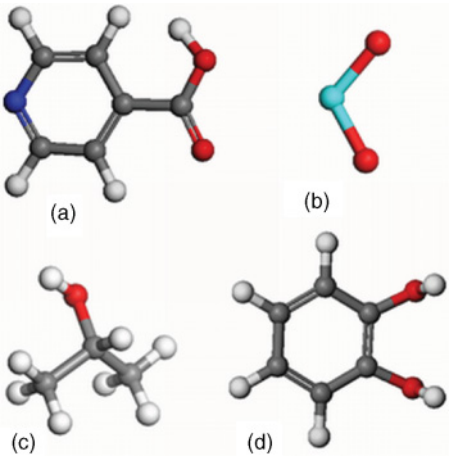

FIG. 2. (Color online) Schematic illustrations of (a) INA, (b) TiO_2, (c) IPA, and (d) catechol.

computed from equilibrium geometries should be compared to vertical IP and EA. However, for some of the systems studied here, only adiabatic experimental values are available. Often the addition or removal of an electron results in a minor structural relaxation such that the adiabatic values are not very far from the vertical values and can still provide a sense of whether a reasonable agreement with the experiment is achieved.

G_0W_0 calculations have been shown to be adequately converged at the tier 4 level, as compared to reference calculations using larger basis sets augmented with Gaussian basis functions and to experimental vertical IPs for a set of small molecules.[32] For TiO_2[38,39] and IPA,[40] the GW@PBEh HOMO and LUMO at the tier 4 level are within 0.1 eV of the experimental IP and EA. For catechol,[41] the GW@PBEh HOMO is very close to the adiabatic IP and about 0.4 eV above the vertical IP.[42] The GW@PBE HOMO and LUMO follow the same basis set convergence trends as those of GW@PBEh. However, they are generally not as close to the experimental IP and EA. This reflects the sensitivity of G_0W_0 calculations to the DFT starting point, elaborated below. Our findings are consistent with those reported for other small organic molecules[32] and for copper phthalocyanine (CuPc).[43]

B. Starting Point Sensitivity

Because the G_0W_0 QP energies are calculated in a "one-shot" non-self-consistent manner, based on the DFT eigenvalues and orbitals, some dependence on the starting point is expected. The starting point dependence of G_0W_0 calculations may enter through the DFT orbitals, whose spatial distribution (e.g., the degree of localization/delocalization) and hybridization may vary, or through the DFT eigenvalues. The question of what is the appropriate starting point for G_0W_0 calculations has been raised before, mostly in the context of narrow-gap semiconductors, which semilocal functionals predict to be metallic, or in the context of wide-gap semiconductors whose band gaps are severely underestimated by semilocal functionals.[44] It has also been shown that for CuPc there is a qualitative difference between the semilocal and hybrid DFT spectra, which stems from the SIE affecting highly localized metal-derived orbitals.[13] This carries over to

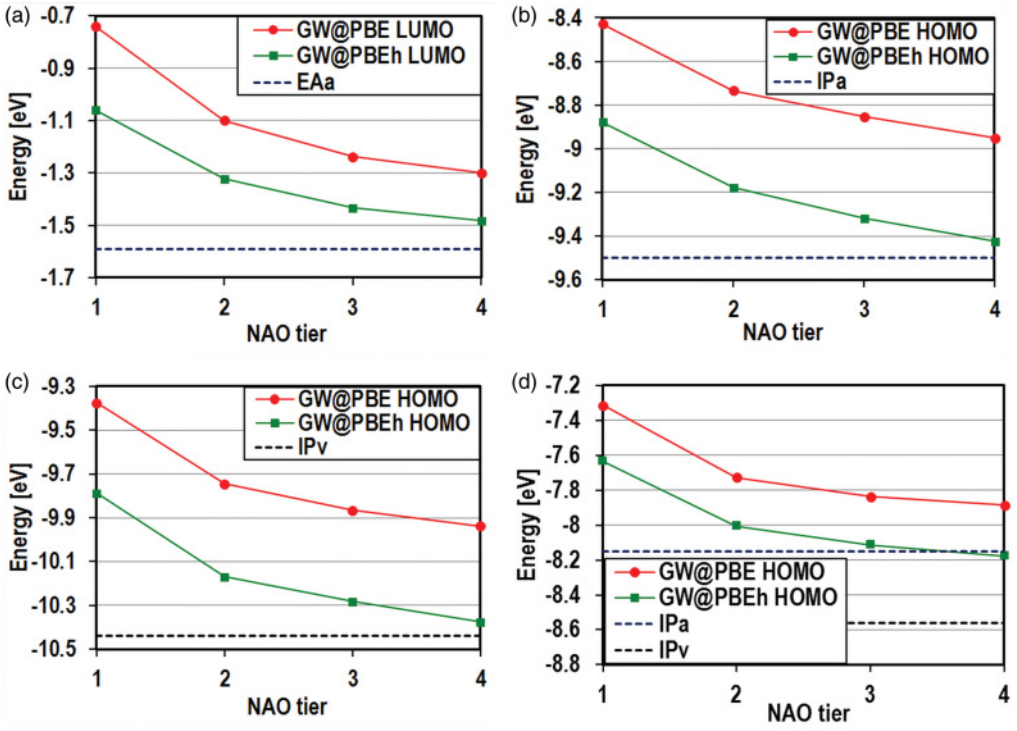

FIG. 3. (Color online) QP HOMO and LUMO energies, calculated based on PBE and PBEh with increasingly large basis sets, compared to experimental IP and EA for (a) and (b) TiO_2,[38,39] (c) IPA,[40] and (d) catechol.[41]

G_0W_0 calculations, leading to qualitative differences between GW@PBE and GW@PBEh in the ordering of the frontier orbitals.[43] For this reason, we now examine the dependence of the QP energies of TiO_2, catechol, and INA on the fraction of exact exchange in the underlying DFT calculation. Figure 4 shows the DFT and QP HOMO and LUMO energies of a TiO_2 molecule, IPA, and catechol, calculated with a tier 4 basis set, using PBE with an increasingly large fraction of exact exchange, as well as HF, and compared to experimental values of IP and EA. We note that the difference between the PBE+100% Exx and the HF starting points is the absence of correlation in the latter. The corresponding IP and EA obtained from total energy differences at the DFT level (ΔSCF) with a tier 2 basis set are also shown for comparison.

We observe that the QP HOMO and LUMO levels remain within 1 eV of the experimental IP and EA, while the corresponding DFT HOMO and LUMO vary by up to 7 eV. We note that the single-particle KS eigenvalues generated using popular DFT functionals are not expected to quantitatively agree with the IP and EA in practice, although in principle there is such a correspondence for the HOMO if the exact DFT functional is used.[45] The ΔSCF values are generally quite close to the G_0W_0 values and can be used in order to shift DFT spectra for the purpose of comparison to photoelectron spectroscopy experiments,[46] as done below.

Interestingly, it is evident from Fig. 4 that the fraction of exact exchange required in order to achieve the best agreement with the experimental IP and EA may vary from one system to another.[47] It has been shown that GW@PBEh gives smaller errors than GW@HF and GW@PBE with respect to the vertical IPs for a set of atoms and molecules.[32] Moreover, in some cases the effect of using a PBEh starting point is more complex than a rigid shift of the QP energies.[43] It is therefore desirable to develop guidelines for choosing the optimal starting point for a G_0W_0 calculation. We attempt to do so by examining the effect of the DFT starting point on the valence QP spectra of $(TiO_2)^-$, catechol, and INA.

Figure 5 shows the DFT and QP spectra of $(TiO_2)^-$, broadened by a 0.25 eV Gaussian to simulate experimental resolution, compared to the gas phase ultraviolet photoemission spectrum (UPS).[39] The DFT spectra are shifted to align the HOMO with the vertical electron detachment energies obtained by taking the total energy difference between the anion and the neutral in the anion geometry with the respective functional. QP energies are directly comparable to gas phase UPS; therefore, they are not shifted. We also note that when comparing the calculated spectra to photoemission experiments, we focus primarily on the peak positions because the peak intensity is also determined by cross-section effects, which our calculations do not include.[48] The semilocal (PBE) and hybrid (PBEh) spectra of $(TiO_2)^-$ are qualitatively similar, and a simple "stretch" of the semilocal spectrum will bring them into close agreement. The G_0W_0 spectra obtained from these two starting points are also qualitatively similar. However, the GW@PBE spectrum is still too compressed, while GW@PBEh spectrum is in close agreement with experiment. GW@PBEh has also yielded excellent agreement with experiment for $(TiO_2)_{2-10}$ clusters.[49]

Figure 6 shows DFT and QP spectra of catechol, broadened by a 0.35 eV Gaussian to simulate experimental resolution, compared to the gas phase UPS of catechol.[41] The DFT spectra are shifted to align the HOMO with the vertical

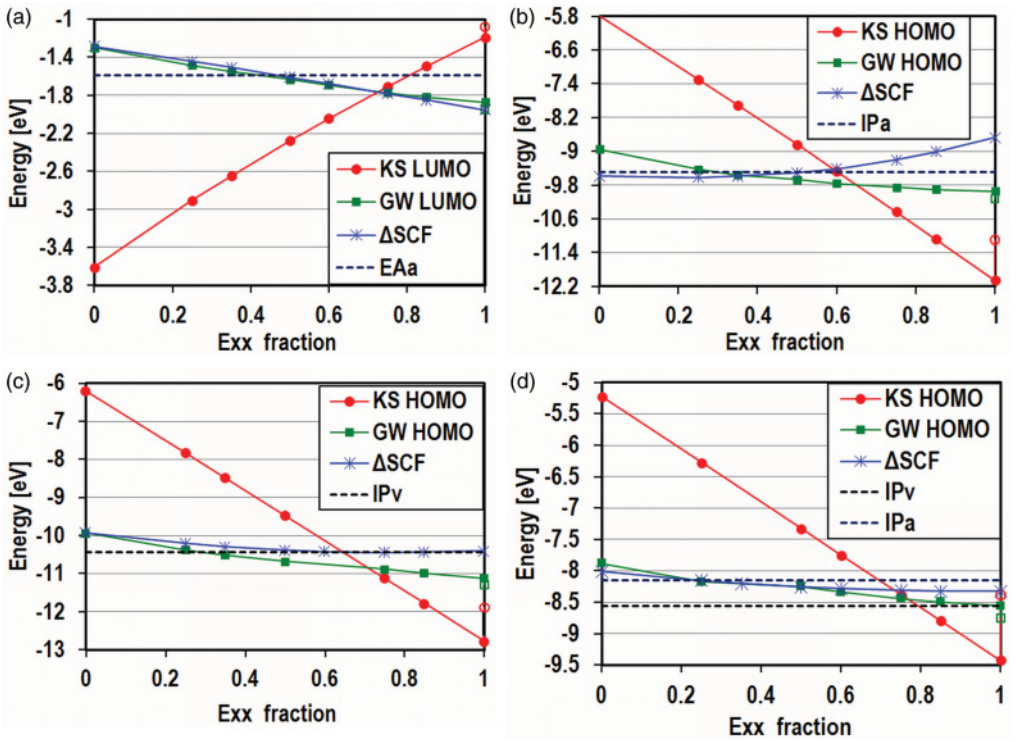

FIG. 4. (Color online) DFT and QP HOMO and LUMO energies, calculated with PBE combined with an increasingly large fraction of exact exchange, and with a tier 4 basis set, compared to experimental IP and EA for (a) and (b) TiO_2,[38,39] (c) IPA,[40] and (d) catechol.[41] The unfilled markers are for HF. The corresponding ΔSCF values obtained at the DFT level with a tier 2 basis set are also shown.

IP obtained by taking the total energy difference between the cation and the neutral in the neutral geometry with the respective functional. QP energies are directly comparable to gas phase UPS; therefore, they are not shifted. As in the case of $(TiO_2)^-$, the semilocal (PBE) and hybrid (PBEh) spectra of catechol are qualitatively similar and a simple "stretch" of the semilocal spectrum will bring them into close agreement. G_0W_0 based on both starting points visibly improves the

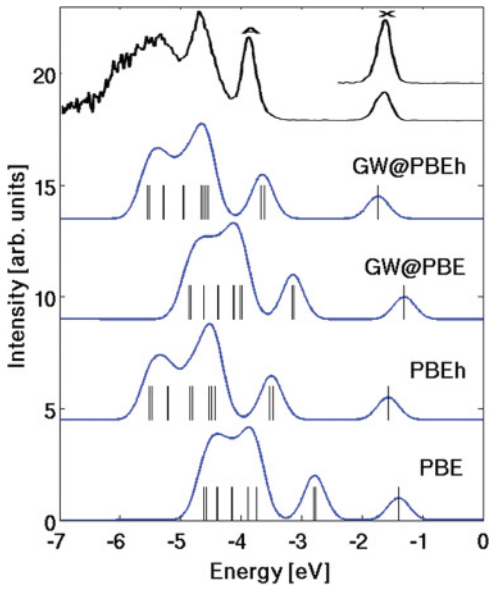

FIG. 5. (Color online) DFT and QP spectra of $(TiO_2)^-$, broadened by a 0.25 eV Gaussian to simulate experimental resolution, compared to gas phase UPS.[39]

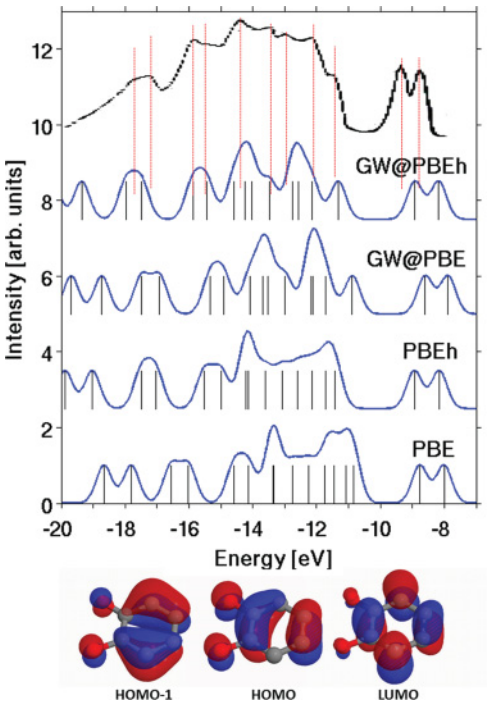

FIG. 6. (Color online) DFT and QP spectra of catechol, broadened by a 0.35 eV Gaussian to simulate experimental resolution, compared to gas phase UPS.[41] Also shown are visualizations of the frontier orbitals of catechol, obtained with PBEh.

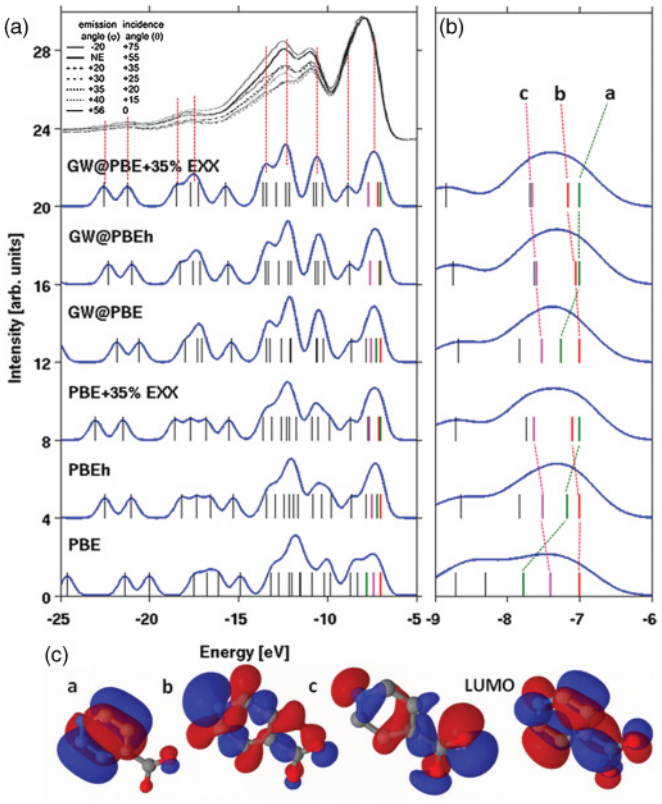

FIG. 7. (Color online) (a) DFT and QP spectra of INA, broadened by a 0.5 eV Gaussian to simulate experimental resolution, compared to the UPS of a monolayer of INA on TiO_2(110).[50] The computed spectra are shifted to align the HOMO level with the experiment. (b) A close-up of the first peak. (c) Visualizations of the frontier orbitals of INA, obtained with PBE+35%Exx.

agreement with experiment. The G_0W_0 spectra obtained from these two starting points are similar. However, the quantitative agreement of the *GW*@PBEh spectrum with experiment is somewhat better than that of *GW*@PBE. A visualization of the molecular orbitals (obtained with PBEh) shows that there are no changes in orbital ordering from PBE to PBEh and from DFT to *GW*.

Both $(TiO_2)^-$ and catechol are typical "well behaved" systems. In the absence of severe SIE effects G_0W_0 is fairly robust to the DFT starting point, and a semilocal starting point is qualitatively adequate. Yet, as is evident from Figs. 4–6, a hybrid starting point gives a better quantitative agreement with experimental electron removal energies.

The case of INA is more complicated. Figure 7(a) shows DFT and QP spectra of INA, broadened by a 0.5 eV Gaussian to simulate experimental resolution, compared to the UPS of a monolayer of INA on TiO_2(110).[41,50] Single-molecule QP energies can be directly and quantitatively compared to gas phase UPS. However, this is not the case for the comparison to an experiment performed on a monolayer because the screening from other surrounding molecules typically causes a uniform shift in the electron removal energies. In order to compensate for this, all the computed spectra are shifted to align the HOMO level with the first UPS peak for the purpose of comparison to experiment. A close-up of the first peak is shown in Fig. 7(b); the frontier orbitals of INA, obtained with PBEh, are visualized in Fig. 7(c).

Although the spectra (both DFT and G_0W_0) calculated with an increasingly large fraction of exact exchange may seem similar at first glance, especially after broadening, a closer look at the molecular orbitals reveals some qualitative differences. For INA, unlike the case of catechol, adding a fraction of exact exchange to PBE leads to changes in the ordering of the frontier orbitals: with PBE, orbital b is the HOMO, orbital c is the HOMO-1, and orbital a is the HOMO-2; with PBEh, orbital b is the HOMO, orbital a is the HOMO-1, and orbital c is the HOMO-2; and with PBE+35%Exx, orbital a is the HOMO, orbital b is the HOMO-1, and orbital c is the HOMO-2. Adding a higher fraction of exact exchange does not lead to any further changes in the orbital ordering. Similarly to the case of CuPc,[43] these differences persist in G_0W_0 calculations based on different starting points: with *GW*@PBE, orbital b is the HOMO, orbital a is the HOMO-1, and orbital c is the HOMO-2; with *GW*@PBEh, orbital a is the HOMO, but it is very close in energy to orbital b, which is the HOMO-1, and orbital c is the HOMO-2; and with *GW*@PBE+35%Exx, orbital a is the HOMO, orbital b is the HOMO-1, and orbital c is the HOMO-2. It is worth noting that although the reordering of orbitals that are close in energy does not affect the shape of the broadened spectrum, it may affect, e.g., the nature of excitations in INA and the subsequent charge transfer to TiO_2, owing to differences in the symmetry and spatial distribution of these orbitals.

Table I shows the *GW* corrections to the DFT energies of orbitals a, b, and c for different fractions of exact exchange. The magnitude of the *GW* correction to the PBE energy of orbital a is significantly lower, by about 0.5 eV, than those of orbitals b and c. For *GW*@PBEh, the magnitude of the correction to the energy of orbital a is still lower by about 0.2 eV than those of orbitals b and c. When PBE+35%Exx is used as a starting point, the *GW* corrections to the DFT energies of all three orbitals are similar. The magnitude of the *GW* correction to the DFT eigenvalues is associated with SIE.[43] This indicates that for PBE, orbitals b and c carry larger SIE than orbital a, resulting from the localization of the nitrogen lone pair. Consequently, their energies are shifted down more than that of orbital a in the G_0W_0 calculation. However, they are not shifted far enough to get the correct orbital ordering. Starting the G_0W_0 calculation from PBEh improves the situation to the point in which the correct orbital ordering is obtained. However, *GW*@PBEh puts orbitals a and b almost on top of each other. When *GW*@PBE+35%Exx is used, the corrections for all three orbitals even out, giving not only the correct orbital ordering but also a bigger spacing between the energies of orbitals a and b. This indicates that *GW*@PBE+35%Exx is a good starting point for INA.

TABLE I. *GW* corrections to the DFT energies [E(QP)-E(DFT)] of the frontier orbitals of INA for different fractions of exact exchange.

Orbital	*GW*@PBE	*GW*@PBEh	*GW*@PBE+35%Exx
a	−2.54	−1.83	−1.51
b	−3.07	−2.03	−1.57
c	−3.19	−2.08	−1.54

The case of INA is reminiscent of other SIE-prone molecules, for which, at the DFT level, hybrid functionals offer a significant qualitative improvement over semilocal functionals.[13,14,43,51] A similar issue has been reported recently for orbitals associated with the nitrogen lone pair of cytosine and uracil.[52] Many dye molecules contain localizing sites, such as transition metal atoms; therefore, they are likely to belong to this category. Errors in the ordering of the frontier orbitals of dyes, particularly in the identities of the HOMO and LUMO, may adversely affect the accuracy of the calculated spectra. In such cases it is particularly important to use an optimal starting point for G_0W_0 calculations and for subsequent BSE calculations. We suggest that the fraction of exact exchange at which there is no further reordering of frontier orbitals, if such a fraction exists, would be a good starting point for G_0W_0.

C. Ti_2cat_2 and Ti_3INA_3

Owing to the size of Ti_2cat_2 and Ti_3INA_3, G_0W_0 calculations were carried out for an isolated molecular unit rather than for the periodic crystal with multiple molecular units per unit cell. Because the units of Ti_2cat_2 and Ti_3INA_3 interact via weak dispersion forces, a periodic treatment is expected to have little consequence for the electronic structure at the dye-TiO_2 interface. For molecular crystals screening effects result primarily in a rigid shift of the QP energies. The unit geometry was obtained via full unit cell relaxation using PBE+TS-vdW, as described in Appendix. In order to isolate the contribution of the dye from that of the IPA, which is not a typical component of a DSC, the calculations were performed with and without the IPA moieties. In order to preserve the Ti coordination, the IPA oxygen was kept and passivated with hydrogen. The G_0W_0 calculations for the systems without IPA (40 atoms for Ti_2cat_2 and 57 atoms for Ti_3INA_3) were performed with a tier 4 basis set. The larger calculations, including the IPA (94 atoms for Ti_2cat_2 and 120 atoms for Ti_3INA_3), were performed with a tier 2 basis set. The QP spectra obtained at the tier 2 level qualitatively resemble those obtained at the tier 4 level because the basis set truncation error is predominantly a uniform shift of 0.2-0.3 eV (see Refs. 32 and 43 and Fig. 3).

In the context of DSCs, we are primarily interested in the level alignment of the dye with respect to the TiO_2. We first discuss the Ti_2cat_2 and Ti_3INA_3 clusters without IPA. The level alignment of catechol with respect to Ti_2cat_2 without IPA, obtained using DFT and G_0W_0, is shown in Fig. 8. Visualization of the DFT orbitals, some of which are shown in Fig. 9 (as obtained with PBEh), allows us to determine whether a particular orbital is associated with catechol or with TiO_2 or has mixed contributions from both. Generally, we observe the following: (i) The HOMO–HOMO-1 and HOMO-2–HOMO-3 orbitals of the combined system, associated with the HOMO and HOMO-1 orbitals of catechol, respectively (shown in Fig. 6), lie inside the gap of the TiO_2 cluster (note that here we refer to the fundamental gap, not the optical gap); (ii) The LUMO–LUMO+9 orbitals of the combined system are associated with the TiO_2 cluster; (iii) The LUMO+10 and LUMO+11 orbitals, associated with the catechol LUMO (shown in Fig. 6), lie deep within the unoccupied states of the TiO_2 cluster and are strongly hybridized with TiO_2 states. This

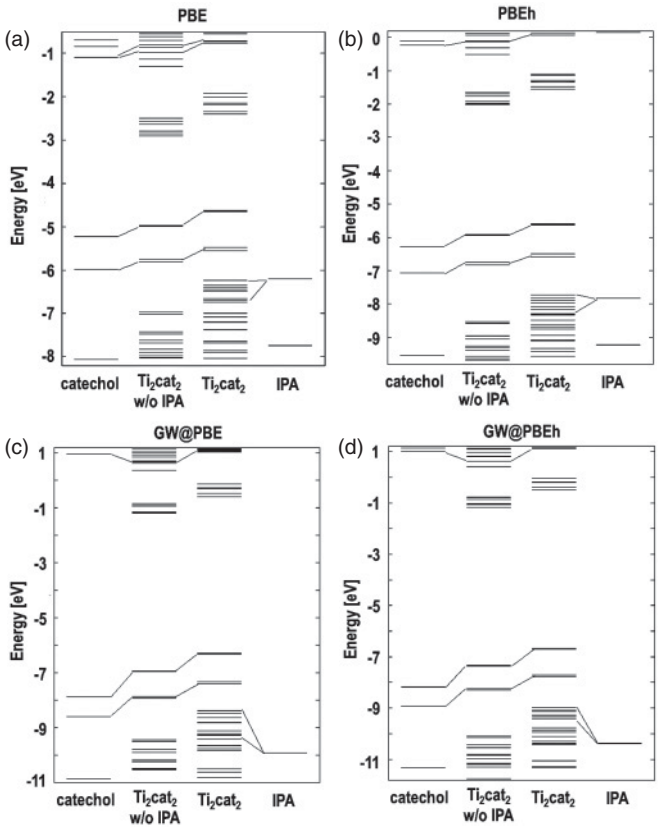

FIG. 8. Level alignment of catechol, IPA, and Ti_2cat_2 with and without IPA, obtained using (a) PBE, (b) PBEh, (c) *GW*@PBE, and (d) *GW*@PBEh.

is the desired level alignment for a DSC, such that an electron may be photoexcited from the catechol HOMO to the catechol LUMO and transferred from there to the TiO_2.

Although the qualitative picture described above is maintained throughout, from PBE to PBEh and from both to GW, the quantitative details of the level alignment change. One obvious difference is that adding exact exchange widens the gap, and using GW widens it further. The position of the catechol HOMO level in the TiO_2 gap also changes. PBE puts the orbital associated with the catechol HOMO in the middle of the TiO_2 gap—2.0 eV above the level associated with the TiO_2 HOMO and 2.1 eV below the TiO_2 LUMO. PBEh puts the catechol HOMO 2.6 eV above the TiO_2 HOMO and 3.9 eV below the TiO_2 LUMO. Here, the G_0W_0 calculations exhibit slight starting point sensitivity as GW@PBE puts the catechol HOMO 2.5 eV above the TiO_2 HOMO and 5.8 eV below the TiO_2 LUMO, while *GW*@PBEh puts the catechol HOMO 2.8 eV above the TiO_2 HOMO and 6.2 eV below the TiO_2 LUMO. Another difference is the absolute position of the catechol LUMO, which is bound in DFT but above the vacuum level in GW, giving a qualitatively different picture. Accounting for electron-hole interactions should effectively rebind the LUMO level, similarly to benzene.[23] This may be examined in future BSE calculations.

The level alignment of catechol and IPA with respect to Ti_2cat_2 is also shown in Fig. 8. We note that because the calculations for Ti_2cat_2 were conducted with a tier 2 basis set, an upward shift of the QP energies by about 0.2 eV on

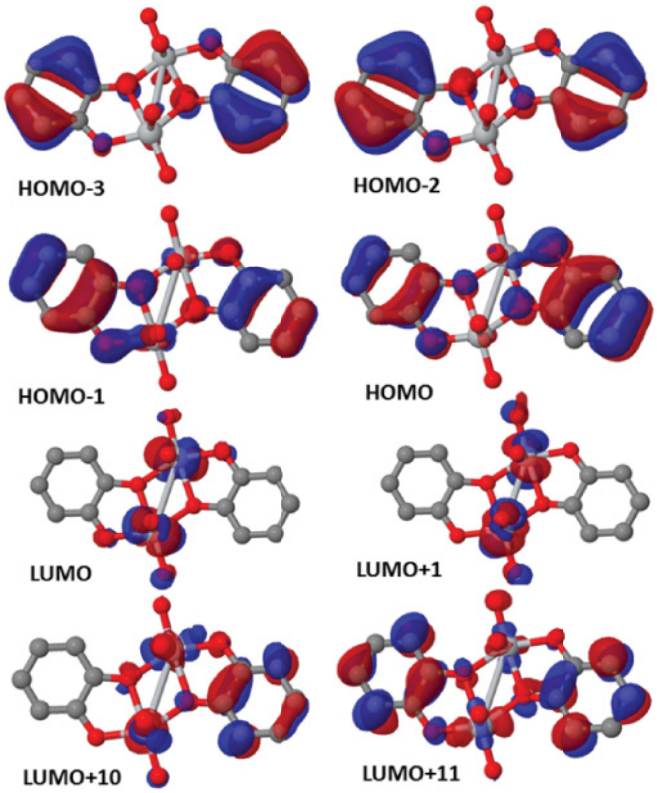

FIG. 9. (Color online) Frontier orbitals of Ti_2cat_2 without IPA, obtained with PBEh.

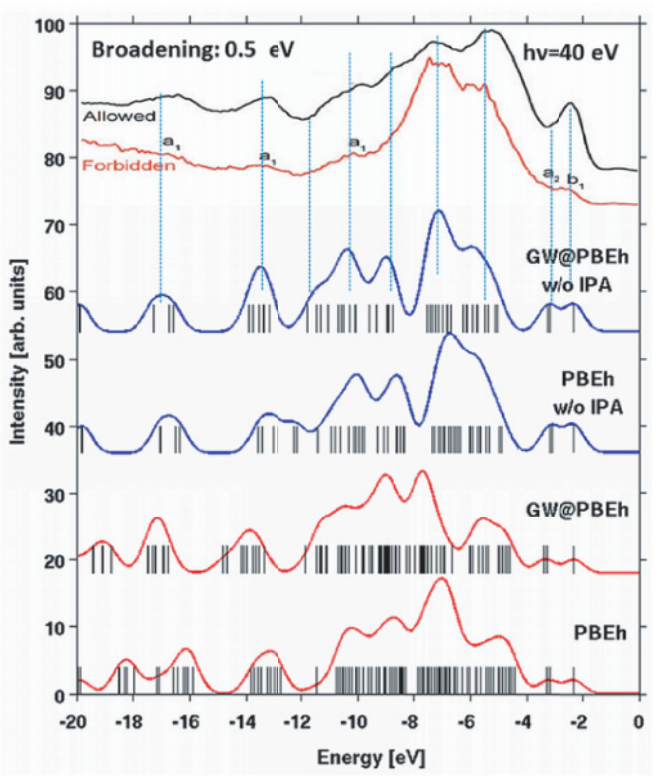

FIG. 10. (Color online) DFT and QP spectra of Ti_2cat_2, with and without IPA, broadened by a 0.5 eV Gaussian to simulate experimental resolution, compared to the UPS of a monolayer of catechol on TiO_2(110), taken at two polarizations.[53] The computed spectra are shifted to align the HOMO level with the experiment.

average is expected (see Fig. 3 and Refs. 32 and 43). Using a larger basis set will not change the picture regarding the effect of IPA. At the DFT level, the IPA HOMO lies deep below the catechol HOMO, and the IPA LUMO lies high above the catechol LUMO. G_0W_0 pushes the IPA HOMO even further down. In this case, the addition of IPA does not change the picture described above and thus has no implication for the photoexcitation of catechol and the subsequent charge transfer to the TiO_2.

Figure 10 shows DFT and QP spectra of Ti_2cat_2, with and without IPA, broadened by a 0.5 eV Gaussian to simulate experimental resolution, compared to the UPS of a monolayer of catechol on TiO_2(110), taken at two polarizations.[53] The computed spectra are shifted to align the HOMO level with the experiment. Similarly to the catechol molecule, whose signature is the dominant component of this spectrum, the GW@PBEh spectrum of the system without IPA is in very good agreement with experiment, offering a slight improvement over PBEh, which is also in good agreement with experiment, at least at the presently available resolution. The addition of IPA changes the shape of the spectrum although the signature of catechol is still clearly visible. The spectrum of Ti_2cat_2 may be compared directly to a UPS experiment for that system when such data become available.

In the case of Ti_3INA_3, as expected based on our findings for INA, there is a greater starting point sensitivity, not only in the level alignment, shown in Fig. 11, but also in the nature of the frontier orbitals, shown in Fig. 12 (as obtained with PBE and PBE+35%Exx). The predictions of PBE, PBE+35%Exx, GW@PBE, and GW@PBE+35%Exx are qualitatively different. We begin by discussing the Ti_3INA_3 cluster without IPA. PBE places the orbital associated with the INA HOMO 0.8 eV above the orbital associated with the TiO_2 HOMO and 2.3 eV below the LUMO. Visualization of the frontier orbitals shows that the HOMO–HOMO-2 orbitals of the combined system are associated with orbital b of INA [Fig. 12(b)] and the HOMO-3–HOMO-5 orbitals of the combined system are associated with orbital a of INA [Fig. 12(a)]. The HOMO-6 orbital of the combined system, shown in Fig. 12(c), has mixed contributions from orbitals a and c of INA and from the TiO_2 cluster. GW@PBE gives the same orbital ordering but places the orbital associated with the INA HOMO 0.3 eV above the orbital associated with the TiO_2 HOMO and 6.8 eV below the LUMO.

PBE+35%Exx places the orbital associated with the INA HOMO 0.7 eV above the orbital associated with the TiO_2 HOMO and 5.7 eV below the LUMO. Visualization of the frontier orbitals shows that the HOMO–HOMO-2 orbitals of the combined system are associated with orbital a of INA ([Fig. 12(a)] and the HOMO-3–HOMO-5 orbitals of the combined system are associated with orbital b of INA [Fig. 12(b)]. The HOMO-6 [Fig. 12(d)] and HOMO-7 orbitals of the combined system are associated with the HOMO-3 orbital from the PBE+35%Exx. The HOMO-8 orbital has mixed contributions from orbital c of INA and from the TiO_2 cluster. GW@PBE+35%Exx gives the same orbital ordering but places the orbital associated with the INA HOMO 0.6 eV

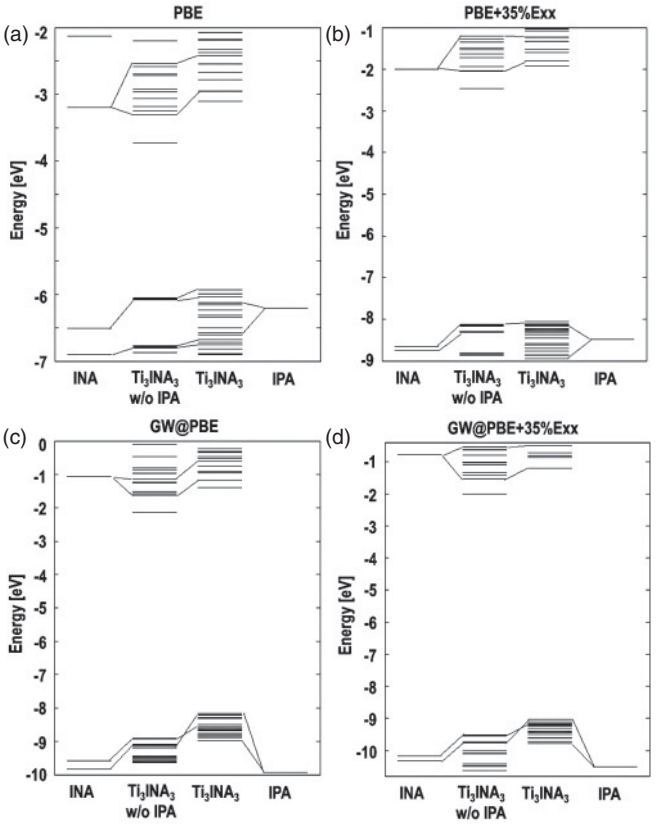

FIG. 11. Level alignment of INA, IPA, and Ti_3INA_3 with and without IPA, obtained using (a) PBE, (b) PBE+35%Exx, (c) *GW*@PBE, and (d) *GW*@PBE+35%Exx.

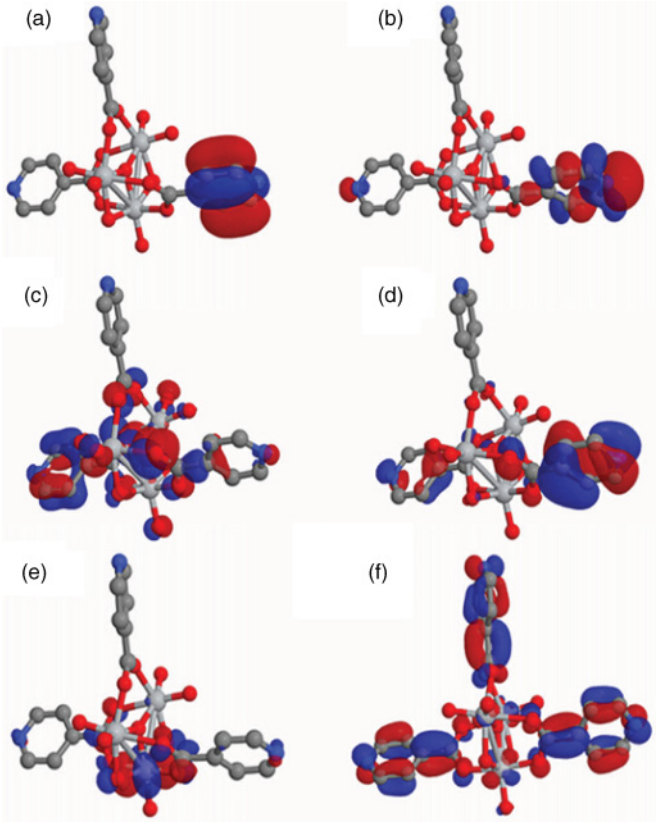

FIG. 12. (Color online) Frontier orbitals of Ti_3INA_3 without IPA, obtained with PBE and PBE+35%Exx: (a) orbital associated with INA a orbital, (b) orbital associated with INA b orbital, (c) PBE HOMO-6, (d) PBE+35% Exx HOMO-6, (e) orbital associated with TiO_2 LUMO, and (f) orbital associated with INA LUMO.

above the orbital associated with the TiO_2 HOMO and 7.5 eV below the LUMO.

In all calculations the LUMO of the combined system, shown in Fig. 12(e), is associated with the TiO_2 cluster. The INA LUMO is highly hybridized with the TiO_2 orbitals and has contributions to orbitals as low as LUMO+1 and as high as LUMO+10. The orbitals with the strongest contributions from the INA LUMO (such an orbital is shown in Fig. 12(f) are the LUMO+8 and LUMO+9 for PBE and the LUMO+7 for PBE+35%Exx. These orbitals are found 1.0 eV above the LUMO with PBE and PBE+35%Exx and 1.2 eV and 1.4 eV above the LUMO with *GW*@PBE and *GW*@PBE+35%Exx, respectively. As it pertains to DSCs, the level alignment of Ti_3INA_3 is somewhat less ideal than that of Ti_2cat_2. The INA HOMO is very close to the TiO_2 HOMO, so there is little to gain by photoexciting the INA rather than the TiO_2. The INA LUMO and TiO_2 LUMO are too close to reasonably speculate on relative energies of photoexcited states on INA and charge transfer with the TiO_2 cluster without explicitly accounting for excitonic effects.

The level alignment of INA and IPA with respect to Ti_3INA_3 is also shown in Fig. 11. We note that because the calculations for Ti_3INA_3 were conducted with a tier 2 basis set, the QP energies are shifted upward by about 0.2 eV on average (see Fig. 3 and Refs. 32 and 43). Using a larger basis set will not change the picture regarding the effect of IPA. In the case of Ti_3INA_3 the addition of IPA complicates the picture. As isolated molecules, the level alignment between INA and IPA is such that DFT places the IPA HOMO above the INA HOMO, while G_0W_0 places the IPA HOMO below the INA HOMO. In addition, the IPA HOMO is close to the TiO_2 HOMO. In the combined system, this leads to the formation of hybridized orbitals with mixed contributions from the frontier orbitals of two or more components. The addition of exact exchange changes the orbital alignment of the three components, resulting in different orbital hybridizations. This causes significant changes in the nature of the orbitals, not just in their ordering.

Figure 13 shows the ordering of the frontier orbitals of Ti_3INA_3 with DFT and *GW*, as well as visualizations of some of these orbitals, obtained with PBE and with PBE+35%Exx. With PBE, as for the system without the IPA, the HOMO–HOMO-2 orbitals of Ti_3INA_3 are associated with INA orbital b. The HOMO-3–HOMO-10 orbitals are associated mainly with the IPA HOMO. The HOMO-11, HOMO-12, and HOMO-14 orbitals are associated with INA orbital a. With PBE+35%Exx, as for the system without the IPA, the HOMO–HOMO-2 orbitals of the combined system are associated with INA orbital a. The HOMO-3–HOMO-12 orbitals are mainly hybridized orbitals comprising contributions from the IPA HOMO mixed with INA orbital b, except for the HOMO-7, which is associated only with INA orbital b.

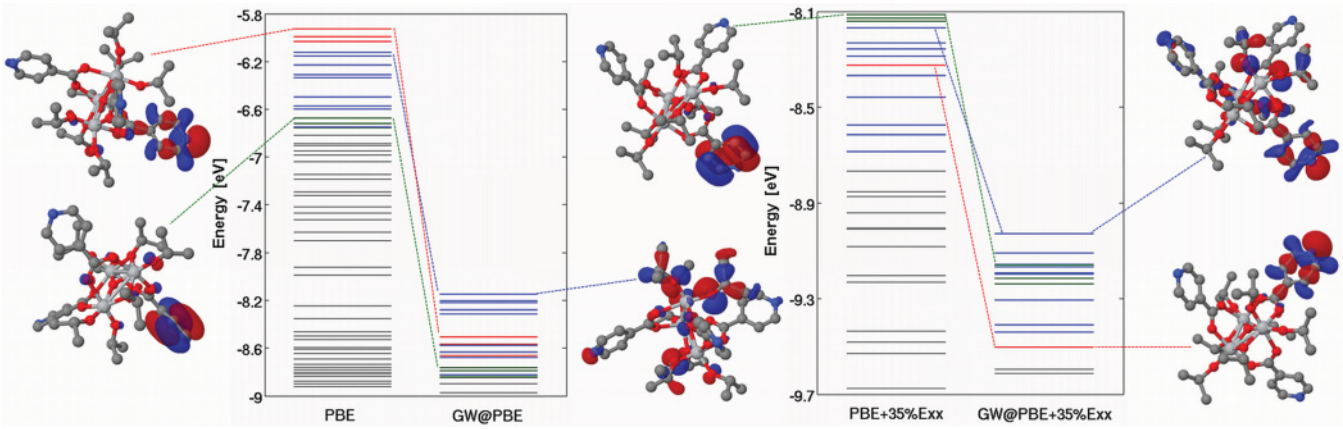

FIG. 13. (Color online) Ordering of the frontier orbitals of Ti_3INA_3 with DFT and *GW*, as obtained with PBE vs PBE+35%Ex. The energy levels of orbitals associated with INA orbital a are marked in green/light gray, the energy levels of orbitals associated with INA orbital b are marked with red/dark gray, and orbitals associated with the IPA HOMO are marked in blue/medium gray.

Contrary to what one would expect based on the level alignment of free INA and IPA molecules, G_0W_0 shifts the orbitals associated with the IPA HOMO to higher energies than those associated with the INA HOMO. With GW@PBE, the HOMO-3–HOMO-7 orbitals rise above the PBE HOMO, and the HOMO-8–HOMO-9 orbitals rise above the PBE HOMO-1. At the same time, the HOMO-11, HOMO-12, and HOMO-13 orbitals, associated with INA orbital a, remain in their relative position below the orbitals associated with INA orbital b. With GW@PBE+35%, the HOMO-3, HOMO-4, and HOMO-8 orbitals rise above the PBE+35%Exx HOMO, while the HOMO-5, HOMO-9, and HOMO-10 orbitals rise above the HOMO-1. Owing to the mixing between IPA and INA orbitals, these orbitals, associated with the IPA HOMO, drag along fragments of INA orbital b to higher energies, making it the HOMO of the combined system. At the same time, the HOMO-7 orbital, associated only with INA orbital b, without contributions from IPA, is not shifted to a higher energy and remains below the orbitals associated with INA orbital a and also below those associated with the IPA HOMO.

This indicates that there is a "conflict of interests" for orbitals with mixed contributions from INA orbital b and the IPA HOMO. The G_0W_0 corrections to the energies of orbitals associated with INA orbital b are more negative than the G_0W_0 corrections to the energies of orbitals associated with the IPA HOMO. However, because there is no self-consistency in the wave function, these orbitals cannot rehybridize. In this case, the results of G_0W_0 calculations are unreliable. We find that the addition of any amount of exact exchange, up to HF, reshuffles the orbitals and leads to a different mixing of the frontier orbitals of INA, IPA, and TiO_2. Performing G_0W_0 on top of any starting point results in shifting of the orbitals associated with the IPA HOMO to higher energies. If these orbitals have mixed contributions from other components of the system, these are dragged along with the IPA HOMO. This demonstrates a failure of the assumption that the DFT wave function is a good approximations to the QP wave function. When hybridization cannot be properly treated by a DFT functional, some level of GW self-consistency is required. This issue will be examined in future work. Barring some uncertainty regarding the orbital ordering, the fact that orbitals associated with IPA lie above orbitals associated with INA indicates that some contributions to the absorption spectrum of Ti_3INA_3 may actually come from IPA rather than INA.

Figure 14 shows the DFT and QP spectra of Ti_3INA_3, with and without IPA, broadened by a 0.5 eV Gaussian to simulate

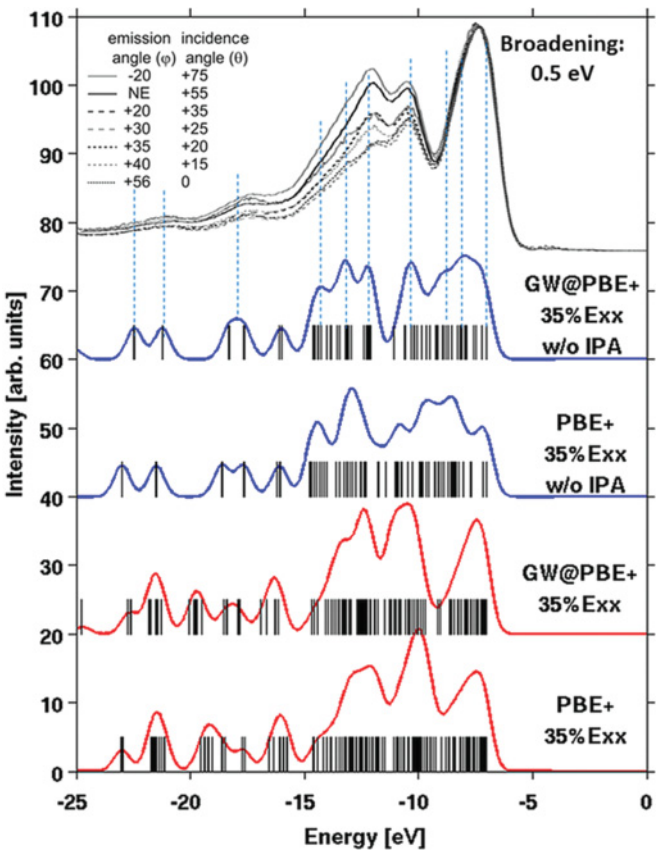

FIG. 14. (Color online) DFT and QP spectra of Ti_3INA_3, with and without IPA, broadened by a 0.5 eV Gaussian to simulate experimental resolution, compared to the UPS of a monolayer of INA on TiO_2(110).[50] The computed spectra are shifted to align the HOMO level with the experiment.

experimental resolution, compared to the UPS of a monolayer of INA on TiO_2(110).[50] The computed spectra are shifted to align the HOMO level with the experiment. Similarly to the INA molecule, whose signature is the dominant component of this spectrum, the GW@PBE+35%Exx spectrum of the system without IPA is in good agreement with experiment, offering a slight improvement over PBE+35%Exx, which is also in good agreement with experiment, at least at the presently available resolution. The addition of IPA changes the shape of the spectrum although the signature of INA is still clearly visible. The changes in the ordering of the frontier orbitals of Ti_3INA_3 are in a dense part of the spectrum, making them impossible to discern at the presently available resolution. The spectrum of Ti_3INA_3 may be compared directly to a UPS experiment for that system, when such data become available.

IV. CONCLUSION

We have conducted a G_0W_0 study of two systems of dye-sensitized TiO_2 clusters, Ti_2cat_2 and Ti_3INA_3. We have demonstrated the following:

(i) Accounting for van der Waals interactions is essential for obtaining geometries in good agreement with experiment.

(ii) The results of hybrid-based G_0W_0 calculations are in good agreement with the positions of resolvable peaks in presently available UPS data.

(iii) Even in cases in which DFT gives the correct qualitative picture, G_0W_0 yields valuable quantitative information on the fundamental gaps and level alignment of the dye molecule and the TiO_2 cluster.

(iv) For Ti_2cat_2, the fundamental level alignment is such that the catechol HOMO lies deep in the TiO_2 gap, almost 3 eV above the TiO_2 HOMO, and the catechol LUMO lies about 2 eV above the TiO_2 LUMO. In principle, such a level alignment is desired for a DSC. The addition of IPA does not change this picture because the IPA HOMO is deep below the catechol HOMO and the IPA LUMO is high above the catechol LUMO.

(v) For Ti_3INA_3, the fundamental level alignment is less ideal because the INA HOMO is only $\sim$0.5 eV above the TiO_2 HOMO, and although the main contribution from the INA LUMO is to an orbital $\sim$1 eV above the TiO_2 LUMO, there are also contributions to much lower orbitals. Accounting for exciton binding energy will be necessary to establish even qualitatively the physics of photoexcitation in this system.

(vi) Care must be taken when choosing the mean-field starting point for G_0W_0 calculations, particularly for systems with localizing groups, which are prone to SIE. As different systems require different fractions of exact exchange, we suggest that the fraction of exact exchange that minimizes the reordering of the molecular orbitals is a good starting point for G_0W_0.

(vii) Care must also be taken in G_0W_0 calculations of multicomponent systems, as orbitals with mixed contributions from different parts of the system, whose energies possess significantly different QP corrections, may need to rehybridize. In such cases, the assumption that the mean-field wave function is a good approximation to the QP wave function breaks down and self-consistency in the wave function may be required.

We may now proceed to GW and BSE calculations of the absorption spectra of such systems. Based on the calculations we have presented here, for systems with over 100 atoms, we expect many-body perturbation theory to become a viable tool for obtaining highly accurate quantitative predictions for realistic systems with relevance to solar cell technology.

ACKNOWLEDGMENTS

We acknowledge support from the National Science Foundation under Grant No. DMR-0941645 and No. OCI-1047997 and from the US Department of Energy under Grant No. DE-SC0001878. Computational resources were provided by the National Energy Research Scientic Computing Center (NERSC) and the Oak Ridge Leadership Computing Facility (OLCF), located in the National Center for Computational Sciences at Oak Ridge National Laboratory. The National Science Foundation provided computational resources through TeraGrid at the Texas Advanced Computing Center (TACC) under Grant No. TG-DMR090026.

APPENDIX: GEOMETRY RELAXATION USING VDW-CORRECTED DFT

As discussed above, it is often the case that the geometry of dye-TiO_2 interfaces is not known exactly. Therefore, computational studies have typically relied on plausible suggested binding geometries whose structure was subsequently optimized using DFT with standard semilocal or hybrid functionals.[7,8] A problematic aspect of this procedure is that conventional DFT functionals, based on semilocal correlation, lack dispersion, which is a long-range electron correlation effect. Dispersion corrections have been shown to be essential for obtaining realistic binding geometries of molecules on metal surfaces,[54] as well as on TiO_2.[55] Although vdW interactions are not expected to affect the covalent bonds between the dye and the TiO_2, they may affect the orientation of the dye with respect to the TiO_2 and stabilize certain binding configurations with respect to others. This is particularly important because the electronic structure of the dye-TiO_2 system has been shown to be sensitive to the binding configuration.[8,53] We employ the

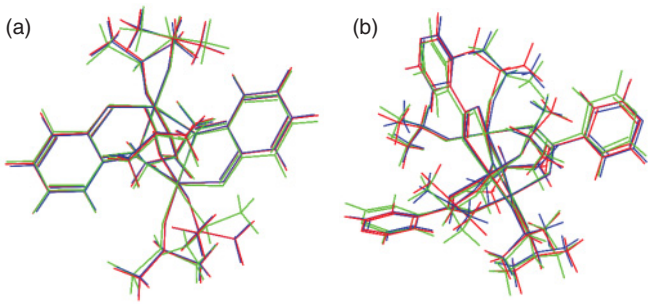

FIG. 15. (Color online) Geometries of (a) Ti_2cat_2 and (b) Ti_3INA_3, obtained using PBE+TS-vdW for isolated clusters (green/light gray) and for the full unit cells (red/dark gray), superimposed on the experimental structure[27] (blue/medium gray).

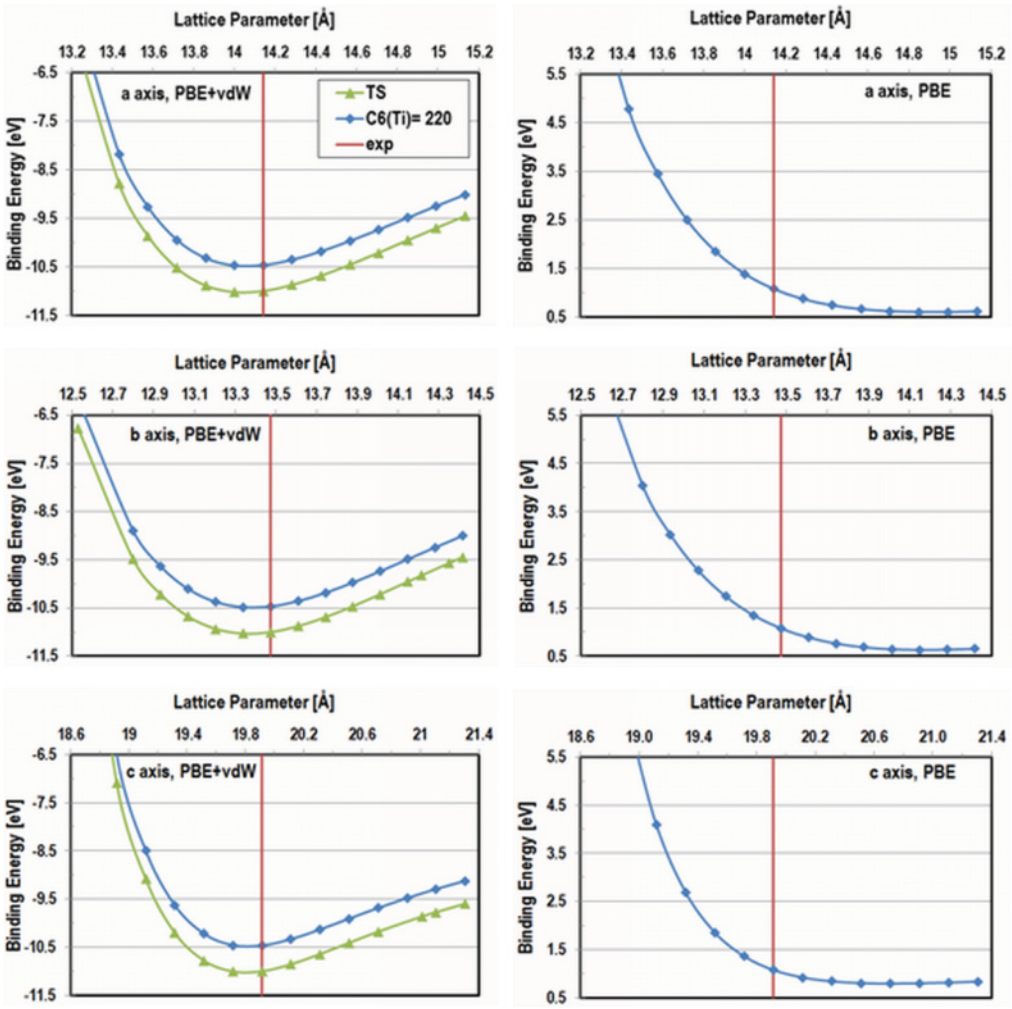

FIG. 16. (Color online) Binding energy curves along the crystal axes of Ti_2cat_2, obtained with and without the TS-vdW correction, compared to the experimental lattice parameters.[27]

TS scheme[31] in order to account for dispersion in the geometry optimization of Ti_2cat_2 and Ti_3INA_3.

In this correction scheme the leading order of the dispersion energy, C_6/R^6, is added in a pairwise manner to the internuclear energy term. The dispersion coefficients, C_6, are determined from Hirshfeld partitioning of the DFT electron density. The Hirshfeld partitioning procedure underestimates ionic charges. This is particularly critical for metal cations, where this leads to significant overestimation of the ionic radii and of the dispersion coefficients. In order to solve this problem, iterative Hirshfeld partitioning[56] has been implemented in FHI-aims. This procedure yields a charge of $+1.2\ e$ on Ti in Ti_3INA_3 and Ti_2cat_2, which corresponds to an estimated C_6 of 220 Hartree·Bohr^6, considerably lower than that of 1440 Hartree·Bohr^6 for neutral Ti.

In order to assess the effect of dispersive interactions with neighboring units on the geometry of the Ti_2cat_2 and Ti_3INA_3 units, geometry relaxation was carried out both for the isolated clusters (with 94 and 120 atoms, respectively) and for the full unit cells (with 376 and 240 atoms, respectively). The latter was performed by relaxing the internal coordinates at the experimental cell parameters of $a = 14.142$ Å, $b = 13.474$ Å, $c = 19.913$ Å, $\alpha = 90°$, $\beta = 115°$, $\gamma = 90°$ for Ti_2cat_2 and $a = 11.739$ Å, $b = 12.886$ Å, $c = 18.312$ Å, $\alpha = 94.758°$, $\beta = 90.202°$, $\gamma = 116.344°$.[27] Figure 15 shows the cluster geometry obtained in isolation and in crystalline form superimposed on the experimental structure. For both clusters better agreement with the experiment is obtained from a fully periodic treatment. This is consistent with the previously reported dependence of the geometry of the repeat unit of β-hematin on weak interactions with adjacent units.[57] In this case, the differences are somewhat less significant than in β-hematin. The geometry of the core TiO_2 clusters is almost unaffected by weak interactions with neighboring units, and the main differences are in the binding geometries of the side groups, particularly the IPA groups, to the TiO_2. For Ti_2cat_2, the periodic treatment results in an excellent agreement with experiment. For Ti_3INA_3 the agreement in the positions of the IPA groups is not as good. This is consistent with the experimentally observed disorder.[27]

In order to demonstrate the importance of the TS-vdW correction for obtaining the correct structure of Ti_2cat_2 and

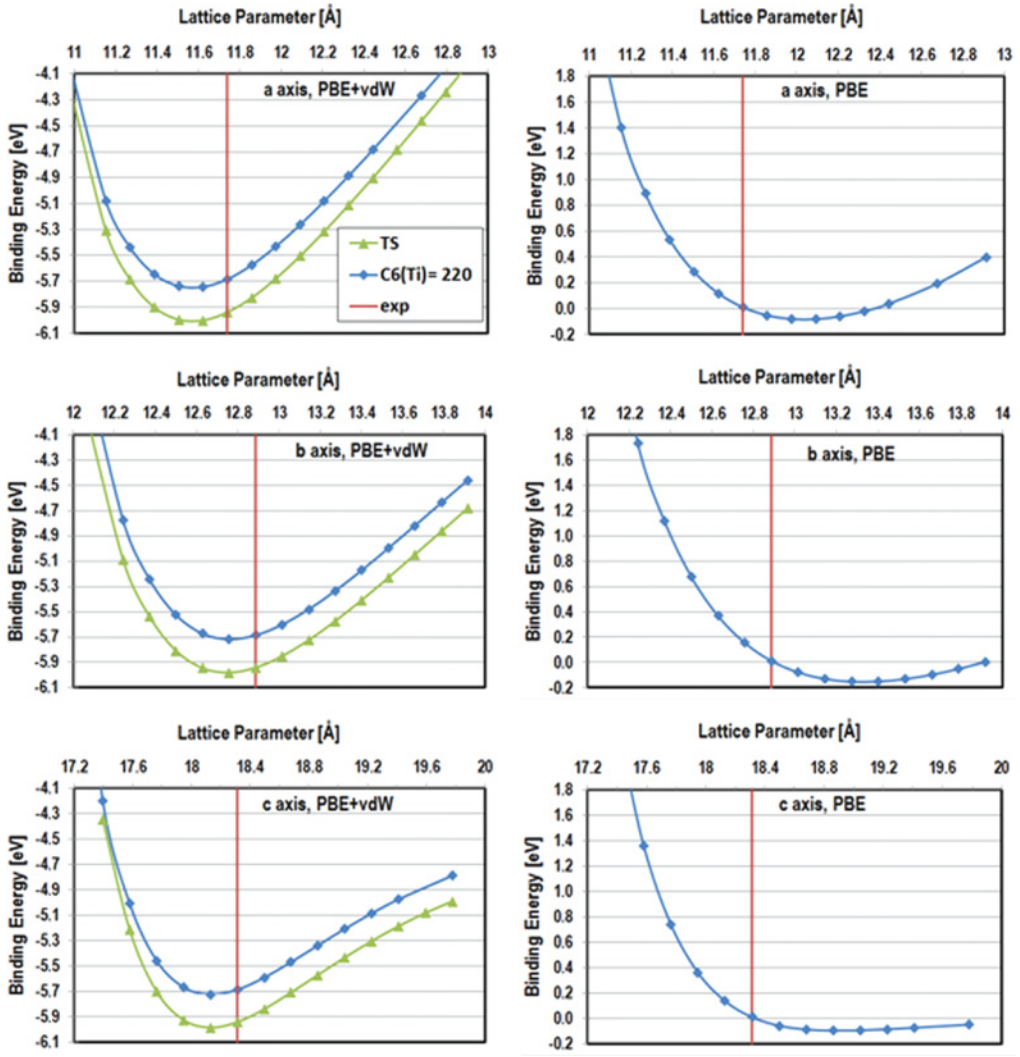

FIG. 17. (Color online) Binding energy curves along the crystal axes of Ti_3INA_3, obtained with and without the TS-vdW correction, compared to the experimental lattice parameters.[27]

Ti_3INA_3, binding energy curves were calculated along the crystal axes with and without the correction. This was done without relaxing the internal coordinates. The binding energies are given with respect to those of relaxed isolated units. The TS-vdW correction was performed both with the standard TS scheme and with the lower C_6 of 220 Hartree·Bohr^6, obtained for Ti using the iterative Hirshfeld method. The results are shown in Figs. 16 and 17, respectively. Clearly, attempting to relax the geometry of such systems without accounting for dispersion would result in structures bearing little resemblance to reality. For Ti_2cat_2, bound only by weak vdW interactions between the catechol and IPA groups of different units, uncorrected PBE gives very shallow minima along all crystal axes and significantly overestimates the lattice parameters. For Ti_3INA_3, uncorrected PBE gives somewhat stronger binding along the *a*- and *b*-axes, where there is a significant contribution from weak CH···N hydrogen bonds between the INA groups of different units [indicated in Fig. 1(b)], although the minimum is still too shallow compared to the vdW-corrected curves, and the lattice parameters are overestimated. Along the c-axis the behavior of uncorrected PBE is similar to that observed for Ti_2cat_2. For both Ti_2cat_2 and Ti_3INA_3, PBE+TS-vdW gives deep minima, and lattice parameters in good agreement with experiment, if slightly underestimated along all crystal axes. The slight underestimation of the lattice parameters may be a result of overestimation of the static polarizability by PBE. Using a C_6 of 220 Hartree·Bohr^6 for Ti leads to a significant reduction in the binding energy comparing to standard TS. However, the geometry is largely unaffected. Using the iterative Hirshfeld procedure to obtain more realistic dispersion coefficients is expected to have a drastic effect for metal-oxide surfaces and other systems comprising a significant portion of metal cations. The success of PBE+TS-vdW in obtaining the geometry of Ti_2cat_2 and Ti_3INA_3 demonstrates yet again the viability of the TS correction scheme for large systems, comprising several hundred atoms.

*noa@ices.utexas.edu

[1] M. Gratzel, Inorg. Chem. **44**, 6841 (2005); Acc. Chem. Res. **42**, 1788 (2009).

[2] A. Hagfeldt, G. Boschloo, L. C. Sun, L. Kloo, and H. Pettersson, Chem. Rev. **110**, 6595 (2010).

[3] G. Hodes, J. Phys. Chem. C **112**, 17778 (2008); O. Niitsoo, S. K. Sarkar, C. Pejoux, S. Ruhle, D. Cahen, and G. Hodes, J. Photochem. Photobiol. A Chem. **181**, 306 (2006); S. K. Sarkar, G. Hodes, L. Kronik, and H. Cohen, J. Phys. Chem. C **112**, 6564 (2008).

[4] Y. M. Cao, Y. Bai, Q. J. Yu, Y. M. Cheng, S. Liu, D. Shi, F. F. Gao, and P. Wang, J. Phys. Chem. C **113**, 6290 (2009).

[5] P. K. Nayak, J. Bisquert, and D. Cahen, Adv. Mater. **23**, 2870 (2011).

[6] D. Jacquemin, E. A. Perpete, G. E. Scuseria, I. Ciofini, and C. Adamo, J. Chem. Theory Comput. **4**, 123 (2008); D. Jacquemin, E. A. Perpete, I. Ciofini, and C. Adamo, Acc. Chem. Res. **42**, 326 (2009); D. Jacquemin, J. Preat, and E. A. Perpete, Chem. Phys. Lett. **410**, 254 (2005); J. F. Guillemoles, V. Barone, L. Joubert, and C. Adamo, J. Phys. Chem. A **106**, 11354 (2002); M. J. Lundqvist, E. Galoppini, G. J. Meyer, and P. Persson, *ibid.* **111**, 1487 (2007); H. Choi, C. Baik, S. O. Kang, J. Ko, M. S. Kang, M. K. Nazeeruddin, and M. Gratzel, Angew. Chem. Int. Ed. Engl. **47**, 327 (2008); M. K. Nazeeruddin, F. De Angelis, S. Fantacci, A. Selloni, G. Viscardi, P. Liska, S. Ito, T. Bessho, and M. Gratzel, J. Am. Chem. Soc. **127**, 16835 (2005); J. E. Monat, J. H. Rodriguez, and J. K. McCusker, J. Phys. Chem. A **106**, 7399 (2002); D. Guillaumont and S. Nakamura, Dyes Pigm. **46**, 85 (2000); R. K. Chen, X. C. Yang, H. N. Tian, X. N. Wang, A. Hagfeldt, and L. C. Sun, Chem. Mater. **19**, 4007 (2007); S. Hayashi, M. Tanaka, H. Hayashi, S. Eu, T. Umeyama, Y. Matano, Y. Araki, and H. Imahori, J. Phys. Chem. C **112**, 15576 (2008); G. Li, K. J. Jiang, Y. F. Li, S. L. Li, and L. M. Yang, *ibid.* **112**, 11591 (2008).

[7] R. Sanchez-de-Armas, J. O. Lopez, M. A. San-Miguel, J. F. Sanz, P. Ordejon, and M. Pruneda, J. Chem. Theory Comput. **6**, 2856 (2010); R. Sanchez-de-Armas, M. A. San-Miguel, J. Oviedo, A. Marquez, and J. F. Sanz, Phys. Chem. Chem. Phys. **13**, 1506 (2011); F. De Angelis, S. Fantacci, and A. Selloni, Nanotechnol. **19**, 424002 (2008); F. De Angelis, S. Fantacci, A. Selloni, M. K. Nazeeruddin, and M. Gratzel, J. Am. Chem. Soc. **129**, 14156 (2007); F. De Angelis, S. Fantacci, E. Mosconi, M. K. Nazeeruddin, and M. Gratzel, J. Phys. Chem. C **115**, 8825 (2011).

[8] M. J. Lundqvist, M. Nilsing, P. Persson, and S. Lunell, Int. J. Quantum Chem. **106**, 3214 (2006); P. Persson and M. J. Lundqvist, J. Phys. Chem. B **109**, 11918 (2005); S. K. Pal, V. Sundstrom, E. Galoppini, and P. Persson, Dalton Trans. (2009) 10021; F. De Angelis, S. Fantacci, A. Selloni, M. Gratzel, and M. K. Nazeeruddin, Nano. Lett. **7**, 3189 (2007); F. De Angelis, S. Fantacci, A. Selloni, M. K. Nazeeruddin, and M. Gratzel, J. Phys. Chem. C **114**, 6054 (2010).

[9] W. R. Duncan and O. V. Prezhdo, J. Phys. Chem. B **109**, 365 (2005).

[10] E. Runge and E. K. U. Gross, Phys. Rev. Lett. **52**, 997 (1984); M. Marques, A. Rubio, C. A. Ullrich, K. Burke, F. Nogueira, and A. Gross, *Time-Dependent Density Functional Theory* (Springer, New York, 2006).

[11] G. Onida, L. Reining, and A. Rubio, Rev. Mod. Phys. **74**, 601 (2002).

[12] J. P. Perdew and A. Zunger, Phys. Rev. B **23**, 5048 (1981); S. Kümmel and L. Kronik, Rev. Mod. Phys. **80**, 3 (2008).

[13] N. Marom, O. Hod, G. E. Scuseria, and L. Kronik, J. Chem. Phys. **128**, 164107 (2008).

[14] N. Marom and L. Kronik, Appl Phys. A Mater. **95**, 159 (2009).

[15] Z.-L. Cai, K. Sendt, and J. R. Reimers, J. Chem. Phys. **117**, 5543 (2002); S. Grimme and M. Parac, Chem. Phys. Chem. **4**, 292 (2003).

[16] A. Dreuw and M. Head-Gordon, J. Am. Chem. Soc. **126**, 4007 (2004); A. Dreuw, J. L. Weisman, and M. Head-Gordon, J. Chem. Phys. **119**, 2943 (2003); D. J. Tozer, *ibid.* **119**, 12697 (2003); T. Ziegler, M. Seth, M. Krykunov, J. Autschbach, and F. Wang, J. Mol. Struct.: Theochem **914**, 106 (2009).

[17] T. Stein, L. Kronik, and R. Baer, J. Chem. Phys. **131**, 244119 (2009).

[18] M. S. Hybertsen and S. G. Louie, Phys. Rev. B **34**, 5390 (1986).

[19] L. Hedin, Phys. Rev. A **139** 796 (1965); F. Aryasetiawan and O. Gunnarsson, Rep. Prog. Phys. **61**, 237 (1998).

[20] M. Rohlfing and S. G. Louie, Phys. Rev. B **62**, 4927 (2000).

[21] N. Sai, M. L. Tiago, J. R. Chelikowsky, and F. A. Reboredo, Phys. Rev. B **77**, 161306 (2008); M. L. Tiago, J. E. Northrup, and S. G. Louie, *ibid.* **67**, 115212 (2003); M. Palummo, C. Hogan, F. Sottile, P. Bagala, and A. Rubio, J. Chem. Phys. **131**, 084102 (2009); M. Rohlfing and S. G. Louie, Phys. Rev. Lett. **82**, 1959 (1999).

[22] J. C. Grossman, M. Rohlfing, L. Mitas, S. G. Louie, and M. L. Cohen, Phys. Rev. Lett. **86**, 472 (2001).

[23] M. L. Tiago and J. R. Chelikowsky, Solid State Commun. **136**, 333 (2005).

[24] L. Chiodo, J. M. Garcia-Lastra, A. Iacomino, S. Ossicini, J. Zhao, H. Petek, and A. Rubio, Phys. Rev. B **82**, 045207 (2010); W. Kang and M. S. Hybertsen, *ibid.* **82**, 085203 (2010); G. Giorgi, M. Palummo, L. Chiodo, and K. Yamashita, *ibid.* **84**, 073404 (2011).

[25] T. Kotani and M. van Schilfgaarde, Phys. Rev. B **81**, 125201 (2010); A. Svane, N. E. Christensen, M. Cardona, A. N. Chantis, M. van Schilfgaarde, and T. Kotani, *ibid.* **81**, 245120 (2010); A. Svane, N. E. Christensen, I. Gorczyca, M. van Schilfgaarde, A. N. Chantis, and T. Kotani, *ibid.* **82**, 115102 (2010); F. Bruneval, Phys. Rev. Lett. **103**, 176403 (2009); F. Bruneval, N. Vast, and L. Reining, Phys. Rev. B **74**, 045102 (2006); C. Rostgaard, K. W. Jacobsen, and K. S. Thygesen, *ibid.* **81**, 085103 (2010); M. Strange, C. Rostgaard, H. Hakkinen, and K. S. Thygesen, *ibid.* **83**, 115108 (2011).

[26] W. Ku and A. G. Eguiluz, Phys. Rev. Lett. **89**, 126401 (2002).

[27] J. B. Benedict and P. Coppens, J. Am. Chem. Soc. **132**, 2938 (2010).

[28] V. Blum, R. Gehrke, F. Hanke, P. Havu, V. Havu, X. Ren, K. Reuter, and M. Scheffler, Comput. Phys. Commun. **180**, 2175 (2009).

[29] V. Havu, V. Blum, P. Havu, and M. Scheffler, J. Comput. Phys. **228**, 8367 (2009).

[30] J. P. Perdew, K. Burke, and M. Ernzerhof, Phys. Rev. Lett. **77**, 3865 (1996); **78**, 1396 (1997).

[31] A. Tkatchenko and M. Scheffler, Phys. Rev. Lett. **102**, 073005 (2009); N. Marom, A. Tkatchenko, M. Scheffler, and L. Kronik, J. Chem. Theory Comput. **6**, 81 (2010); N. Marom, A. Tkatchenko, M. Rossi, V. V. Gobre, O. Hod, M. Scheffler, and L. Kronik, J. Chem. Theory Comput., doi: 10.1021/ct2005616 (2011).

[32] X. Ren, P. Rinke, V. Blum, J. Wieferink, A. Tkatchenko, A. Sanfilipo, K. Reuter, and M. Scheffler, to be published.

[33] H. N. Rojas, R. W. Godby, and R. J. Needs, Phys. Rev. Lett. **74**, 1827 (1995).

[34] R. Gomez-Abal, X. Z. Li, M. Scheffler, and C. Ambrosch-Draxl, Phys. Rev. Lett. **101**, 106404 (2008); C. Friedrich, A. Schindlmayr, S. Blugel, and T. Kotani, Phys. Rev. B **74**, 045104 (2006); M. Shishkin and G. Kresse, *ibid.* **74**, 035101 (2006); M. L. Tiago, S. Ismail-Beigi, and S. G. Louie, *ibid.* **69**, 125212 (2004); M. van Schilfgaarde, T. Kotani, and S. V. Faleev, *ibid.* **74**, 245125 (2006);

W. Ku and A. G. Eguiluz, Phys. Rev. Lett. **93**, 249702 (2004); K. Delaney, P. Garcia-Gonzalez, A. Rubio, P. Rinke, and R. W. Godby, *ibid.* **93**, 249701 (2004); E. Luppi, H. C. Weissker, S. Bottaro, F. Sottile, V. Veniard, L. Reining, and G. Onida, Phys. Rev. B **78**, 245124 (2008).

[35]J. P. Perdew, A. Ruzsinszky, J. M. Tao, V. N. Staroverov, G. E. Scuseria, and G. I. Csonka, J. Chem. Phys. **123**, 062201 (2005); M. Ernzerhof and G. E. Scuseria, *ibid.* **110**, 5029 (1999); C. Adamo and V. Barone, *ibid.* **110**, 6158 (1999).

[36]E. v. Lenthe, E. J. Baerends, and J. G. Snijders, J. Chem. Phys. **101**, 9783 (1994).

[37]B. C. Shih, Y. Xue, P. H. Zhang, M. L. Cohen, and S. G. Louie, Phys. Rev. Lett. **105**, 146401 (2010); C. Friedrich, M. C. Muller, and S. Blugel, Phys. Rev. B **83**, 081101 (2011).

[38]G. Balducci, G. Gigli, and M. Guido, J. Chem. Phys. **83**, 1913 (1985); H. B. Wu and L. S. Wang, *ibid.* **107**, 8221 (1997).

[39]H.-J. Zhai and L.-S. Wang, J. Am. Chem. Soc. **129**, 3022 (2007).

[40]F. M. Benoit and A. G. Harrison, J. Am. Chem. Soc. **99**, 3980 (1977).

[41]M. H. Palmer, W. Moyes, M. Speirs, and J. N. A. Ridyard, J. Mol. Struct. **52**, 293 (1979).

[42]A similar comparison for INA is not conducted here because experimental values for its IP and/or EA are presently unavailable.

[43]N. Marom, X. Ren, J. E. Moussa, J. R. Chelikowsky, and L. Kronik, Phys. Rev. B **84**, 195143 (2011).

[44]H. Jiang, R. I. Gomez-Abal, P. Rinke, and M. Scheffler, Phys. Rev. B **82**, 045108 (2010); A. Qteish, P. Rinke, M. Scheffler, and J. Neugebauer, *ibid.* **74**, 245208 (2006); P. Rinke, A. Qteish, J. Neugebauer, C. Freysoldt, and M. Scheffler, New J. Phys. **7**, 126 (2005); P. Rinke, A. Qteish, J. Neugebauer, and M. Scheffler, Phys. Status Solidi B **245**, 929 (2008); P. Rinke, M. Scheffler, A. Qteish, M. Winkelnkemper, D. Bimberg, and J. Neugebauer, Appl. Phys. Lett. **89**, 161919 (2006); F. Fuchs and F. Bechstedt, Phys. Rev. B **77**, 155107 (2008); C. Rodl, F. Fuchs, J. Furthmuller, and F. Bechstedt, *ibid.* **79**, 235114 (2009).

[45]J. F. Janak, Phys. Rev. B **18**, 7165 (1978).

[46]L. Kronik, R. Fromherz, E. Ko, G. Gantefor, and J. R. Chelikowsky, Nat. Mater. **1**, 49 (2002); M. Moseler, B. Huber, H. Häkkinen, U. Landman, G. Wrigge, M. Astruc Hoffmann, and B. v. Issendorff, Phys. Rev. B **68**, 165413 (2003); O. Guliamov, L. Kronik, and K. A. Jackson, J. Chem. Phys. **123**, 204312 (2005).

[47]We note that tuning the fraction of exact exchange and using a simple hybrid functional as a mean-field starting point often improves upon semilocal DFT; however, it has the limitation that there is no system specific definition of screening. In this respect, the Coulomb-hole plus screened-exchange (COHSEX) approach may be a better albeit more expensive starting point.

[48]M. Vogel, F. Schmitt, J. Sauther, B. Baumann, A. Altenhof, S. Lach, and C. Ziegler, Analytical and Bioanalytical Chemistry **400**, 673 (2011).

[49]N. Marom, M. Kim, and J. R. Chelikowsky, to be published.

[50]J. N. O'Shea, J. C. Swarbrick, K. Nilson, C. Puglia, B. Brena, Y. Luo, and V. R. Dhanak, J. Chem. Phys. **121**, 10203 (2004).

[51]T. Körzdörfer, S. Kümmel, N. Marom, and L. Kronik, Phys. Rev. B **82**, 129903 (2010); **79**, 201205 (2009); D. Stradi, C. Diaz, F. Martin, and M. Alcami, Theor. Chem. Acc. **128**, 497 (2011); T. Körzdörfer, J. Chem. Phys. **134**, 094111 (2011).

[52]C. Faber, C. Attaccalite, V. Olevano, E. Runge, and X. Blase, Phys. Rev. B **83**, 115123 (2011).

[53]S. C. Li, J. G. Wang, P. Jacobson, X. Q. Gong, A. Selloni, and U. Diebold, J. Am. Chem. Soc. **131**, 980 (2009).

[54]E. R. McNellis, J. Meyer, and K. Reuter, Phys. Rev. B **80**, 205414 (2009); K. Tonigold and A. Gross, J. Chem. Phys. **132**, 224701 (2010).

[55]J. P. P. Ramalho and F. Illas, Chem. Phys. Lett. **501**, 379 (2011).

[56]A. Olasz, K. Vanommeslaeghe, A. Krishtal, T. Veszpremi, C. Van Alsenoy, and P. Geerlings, J. Chem. Phys. **127**, 224105 (2007); P. Bultinck, P. W. Ayers, S. Fias, K. Tiels, and C. Van Alsenoy, Chem. Phys. Lett. **444**, 205 (2007); P. Bultinck, C. Van Alsenoy, P. W. Ayers, and R. Carbo-Dorca, J. Chem. Phys. **126**, 144111 (2007).

[57]N. Marom, A. Tkatchenko, S. Kapishnikov, L. Kronik, and L. Leiserowitz, Cryst. Growth Des. **11**, 3332 (2011).